




Photocatalytic performance of textiles coated with titanium dioxide-reduced graphene oxide system for degradation of crude petroleum under similar solar irradiation

Davide Silva¹, Salmon Landi Jr.^{2,*}, Iran Rocha Segundo^{1,3,*} , Cátia Afonso¹, Filipa Fernandes¹, Eloiza da Silva Nunes², Vasco Teixeira¹, Jéferson Aparecido Moreto⁴, and Joaquim Carneiro^{1,*}

¹Centre of Physics of Minho and Porto Universities (CF-UM-UP), University of Minho, Azurém Campus, Guimarães, Portugal

²Federal Institute Goiano, Rio Verde, Goiás, Brazil

³ISISE, Department of Civil Engineering, University of Minho, Azurém Campus, Guimarães, Portugal

⁴Institute of Exact Sciences, Naturals and Education, Federal University of Triângulo Mineiro (UFTM), Uberaba, Minas Gerais, Brazil

Received: 6 August 2021

Accepted: 27 December 2021

Published online:

5 February 2022

© The Author(s), under exclusive licence to Springer Science+Business Media, LLC, part of Springer Nature 2022

ABSTRACT

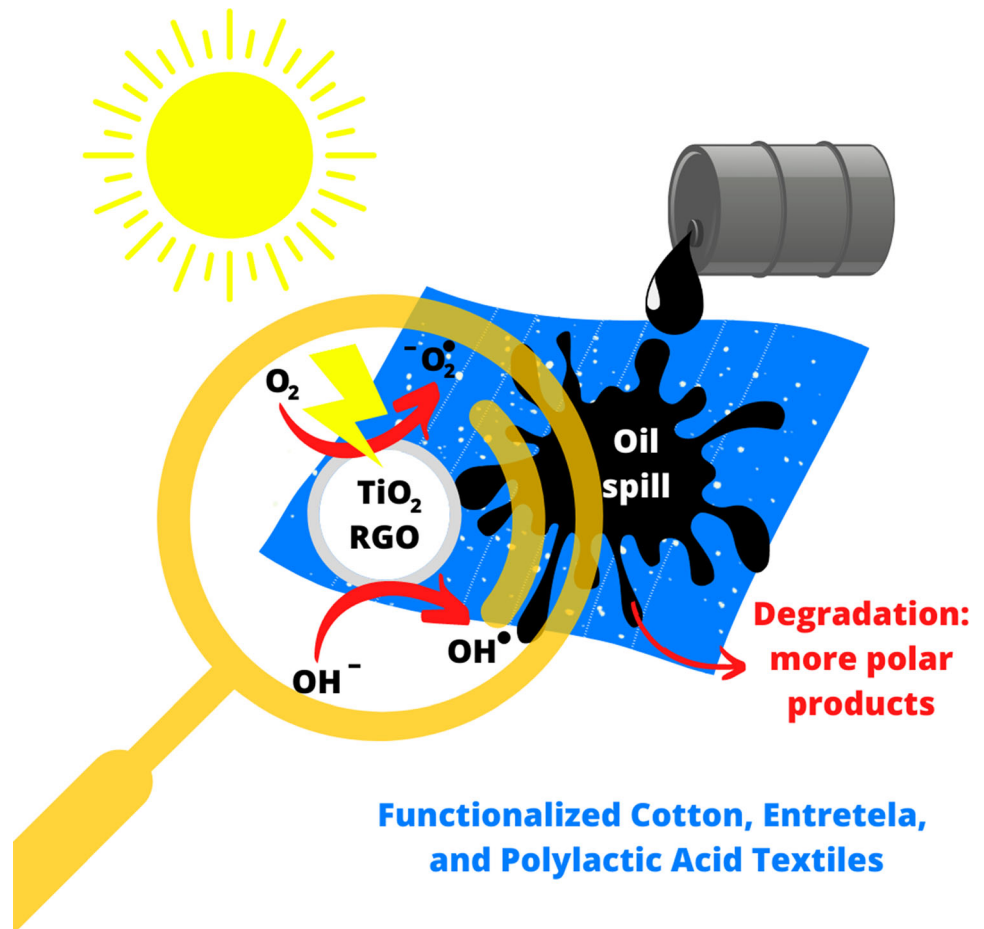
The pollution caused by oil and its toxic derivatives presents a considerable risk to the public health and the environment. This work is devoted to the study of the influence of TiO₂ nanoparticles immobilized on three types of textiles materials (Cotton, Entretela, and Polylactic Acid–PLA) coated with reduced graphene oxide (RGO) to be used for degradation of crude petroleum under simulated solar irradiation. The morphological studies of the functionalized textiles substrates were performed by using Scanning Electron Microscopy and Energy Dispersive X-ray Spectroscopy, which indicated an excellent dispersion and adhesion of nanoparticles of about 60% (atomic %Ti) on the textile fibers covered with RGO after washing. Ultraviolet–visible Diffuse Reflectance spectra suggest a reduction in the band gap energy of TiO₂ up to 2.86 eV due to the presence of RGO. The functionalized textiles presented at least 60% of photocatalytic efficiency measured by Rhodamine B degradation, decreasing less than 12% after the rigorous washing. The excitation/emission Synchronous Fluorescence Spectroscopy and Fourier-transform Infrared spectroscopies demonstrated a great potential for photocatalytic degradation of the functionalized textiles substrates as the appearance of the hydroxyl, carboxyl, and the C–O bands confirm the photoinduced oxidation of the organic compounds implying with high prospects in petroleum and wastewater treatment areas. Moreover, this environmentally friendly, sustainable, and inclusive research work can be

Handling Editor: Maude Jimenez.

Address correspondence to E-mail: salmon.landi@ifgoiano.edu.br; iran_gomes@hotmail.com; carneiro@fisica.uminho.pt

included in clean technologies, contributing to the novel socio-economic model recognized as “Green Recovery”.

GRAPHICAL ABSTRACT



Introduction

Nowadays, it is estimated 1.8 large oil spills per year (> 1000 tons), so that of all the sources that cause water pollution, those related to the oil industry are one of the most problematic [1, 2]. Accidental spills during exploration, refining, transportation, and storage of oil and its derivatives cause very negative economic impacts on a wide range of services and natural resources such as soils, oceans, surface, and groundwater resources [3, 4]. Among all the organic

and inorganic pollutants present in the oil and its derivatives, polycyclic aromatic hydrocarbons (PAHs), which present two or more condensed aromatic rings, have been highlighted. These compounds are hydrophobic, recalcitrant, and mutagenic and carcinogenic, causing a significant negative impact on the environment. In this way, the PAHs appear as a threat to human health and all ecosystems [5–7].

Given the many occurrences of environmental pollution caused by the massive use of oil and its

derivatives, it is necessary to implement actions intended to the study and the developing of new techniques and materials to mitigate the damage caused to the environment. As King et al. [8] presented, some technologies have been employed to remove or degrade the oil and its various constituents. Among the most promising clean technologies, the advanced oxidation processes (AOPs) have been widely tested on a laboratory scale and pointed as an interesting method to purify the oilfield producer water [9]. The AOPs appear as a very efficient method for degrading the recalcitrant pollutant and inexpensive to implement solutions. The great advantage of AOPs, particularly the heterogeneous photocatalysis combining a source of ultraviolet (UV) and/or visible light and a semiconductor material, comes from the fact that it consists of a destructive treatment [10–12]. The organic pollutants suffer not only phase change, such as in adsorption and filtration processes, but they are degraded through a sequence of chemical reactions where the final products can be environmentally innocuous species such as CO_2 , H_2O , and inorganic ions [5, 13–15].

Actually, the use of semiconductor materials reduces the costs of heterogeneous photocatalysis and enables the mineralization of various organic compounds without any additive [14]. Several semiconductors have been used in photocatalytic degradation of environmental contaminants, including titanium dioxide (TiO_2), zinc oxide (ZnO), tungsten oxide (WO_3), tin oxide (SnO_2), zirconium oxide (ZrO_2), cadmium sulfide (CdS), and others [14, 16–23]. Among many semiconductors, TiO_2 has attracted much attention by different research groups [24–28] because it is inexpensive and chemically stable [29, 30]. However, despite the advantages, TiO_2 presents some limitations, such as a wide band gap energy, low surface area, and rapid recombination of electron/hole pairs (e^-/h^+) [31], which implies a low photocatalytic efficiency [32].

On the other hand, the significant increase in the TiO_2 photoactivity has been obtained mainly by (i) doping process [33, 34], (ii) supporting [19, 35], and (iii) coupling with other semiconductors [32, 36] or noble metals [37–39]. Particularly, TiO_2 combined with carbon-based materials are promising for wastewater treatment [40]. In this sense, the addition of graphene oxide (GO) or even reduced graphene oxide (RGO) enables the extension of the absorption range of TiO_2 to the visible region of the

electromagnetic spectrum and also decrease the recombination process of photogenerated charge carriers [26, 28, 41]. Studies developed by Mahmood et al. [42] showed that the photoexcited electrons from the valence band (VB) to the conduction band (CB) of TiO_2 find an intermediate energy level due to the work function of graphene and gets trapped, causing an effective charge separation. This level between the VB and the CB introduced by graphene also reduces the band gap of TiO_2 [42]. TiO_2 -RGO composites have been essentially utilized to investigate the photodegradation of dyes [43–45], gases [46], among others [47].

The use of semiconductors at the nanoscale domain appears as a strategy to promote improvements in photocatalytic properties. However, scenarios in which the release of nanoparticles to the environment may occur should be avoided because, in this way, they can represent sources of further problems for the surrounding ecosystems and human health. Thus, it becomes crucial to immobilize the photocatalysts on supports to avoid/minimize their subsequent release. One immobilization carrier that has been widely used refers to the textiles substrates [48, 49], which are highly cost-effective due to their huge flexibility and low density. Several scientific works have been reported in the literature on the TiO_2 and RGO system over textile substrates for biomedical [50–52] and photocatalytic applications [53, 54].

Here, we studied the photocatalytic performance of three different types of textiles materials functionalized with RGO and TiO_2 -RGO systems to degrade crude petroleum under solar irradiation. To the best of our acknowledgment, this is the first study related to the use of textile materials functionalized with RGO covered with TiO_2 nanoparticles for petroleum degradation, thus having great application perspectives in the field of materials science.

Materials and methods

All chemicals used were of analytical grade. TiO_2 nanoparticles (Aeroxide TiO_2 P25) were purchased from Quimidroga (Spain), Rhodamine B and acetic acid was acquired from Sigma-Aldrich (Portugal), graphene oxide (GO) powders were purchased from Nanoinnova Technologies S.L. (Spain), and sodium dithionite ($\text{Na}_2\text{S}_2\text{O}_4$) was acquired from Merck. GALP Portugal kindly provided the petroleum. The

wetting solution Diadavin ANE (nonionic) was obtained from the ADI Group. Cotton, Entretela, and Polylactic Acid (PLA) are characteristic and specific terms used in the field of the textile industry, and their meanings can be accessed in a textile glossary [55]. The main objective to functionalize these textile substrates is related to their lightweight, flexibility and easy-to-fitting (facilitating their transportation and application to oil-polluted areas such as soils and oceans), low-cost and scalable production (great availability to include them in the market when functionalized). Also, PLA is a biodegradable polymer derived from renewable sources, for example, corn. Since their composition, morphology, and structure are different, in this study, we intended to analyze the best-functionalized textile that will provide the best degradation performance and also dispersion and adhesion of nanoparticles.

Before carrying out the functionalization process, the fabrics (5 cm × 5 cm) were washed with 1.0 g L⁻¹ nonionic detergent solution at 70 °C for 1 h. They were rinsed with an abundant amount of distilled water to remove any impurities. After dried at room temperature, the functionalization of the textiles substrates was carried out according to our previous studies [53]. Initially, a suspension prepared with 1 g of GO and 1 L distilled water was homogenized by sonication during 1 h; posteriorly, the textiles substrates were inserted in this GO suspension for further 1 h. After drying under ambient conditions, the textiles substrates were placed in a solution containing the reducing agent (3.5 g of Na₂S₂O₄ dissolved in 500 mL of distilled water) at 90 °C for 30 min. Samples with different number of RGO coatings (1–3) were obtained repeating the procedure mentioned above. RGO samples were immersed in a solution prepared 4 g of TiO₂ nanoparticles and 1 L of distilled water for a period of 1 min. The pH of the TiO₂ aqueous solution was adjusted at 2.5 using acetic acid. The cotton substrates were then pressed twice under 2 bar pressure with horizontal rollers (9.0 rpm). Samples with different number of TiO₂ coatings (1–2) were obtained repeating the procedure mentioned above. Finally, the prepared substrates were dried in an oven at 100 °C for 10 min. The assigned name to the samples after functionalization was structured as follows: n₁TiO₂-n₂RGO-X, where n₁ (equal to 1 or 2), n₂ (equal to 1, 2 or 3), and X refer to the number of coatings of TiO₂, the number of coatings of RGO and the type of functionalized textile (C = Cotton, E =

Entretela, and P = PLA), respectively. For example, the sample designated “3TiO₂-2RGO-C” indicates to a functionalized cotton textile with the deposition of two coatings of RGO and after three coatings of TiO₂ nanoparticles.

This study is mainly focused on applying the TiO₂-RGO system onto different fabrics for photodegradation of petroleum under similar sunlight irradiation. For this purpose, X-ray powder diffraction (XRD) and Fourier-transform infrared spectroscopy (FTIR) were performed to reveal the crystalline phase composition of TiO₂ nanoparticles and the reduction process of the GO. The morphology of the samples was assessed by using a FEG/SEM microscope with an acceleration voltage of 5 kV. The chemical elements identification was obtained by Energy-dispersive X-ray spectroscopy (EDX) by using the EDAX-Pegasus X4M (EDX/EBSD) analysis system. The EDX measurements were performed in the range of 0–10 kV. Concerning the Ultraviolet–visible (UV–Vis) spectroscopy, we used a SHIMADZU UV-2501 Spectrophotometer equipped with an integrating sphere and analyzed the band gap energy by the Kubelka–Munk model and Tauc plot.

An aqueous solution of Rhodamine B (Rh-B) dye circulating in a homemade photoreactor was used to test the degree of immobilization for the TiO₂-RGO system on textiles materials. In a typical experiment, the dye solution (5.0 ppm) was maintained under magnetic stirring during the whole test time. It was forced to circulate continuously in the reactor by the action of a peristaltic pump at a constant rate, thus allowing a uniform distribution of Rh-B solution over the entire substrate. The light irradiation was artificially provided by a 300 W OSRAM lamp simulating solar radiation, which is commonly used in literature for different purposes [56–60] including for photocatalysis [61–66], and its light spectrum can be found in [56]. More details of this procedure and images of the photoreactor can be found in previous works [53, 67]. The decrease in Rh-B concentration was monitored by UV–visible spectrophotometry over intervals of 0, 40, 80, 120, and 180 min. In these time intervals, aliquots of the dye solution (3 mL) were taken and analyzed by using the SHIMADZU UV-2501 PC UV–Vis Spectrophotometer in a range of wavelengths from 300 to 700 nm. The photodegradation tests for each functionalized substrate were performed before and after five washes to evaluate the immobilization degree of the TiO₂-RGO system

on the textiles substrates. This process induces severe conditions since the washing procedure was performed at a temperature of 60 °C using a distilled water and nonionic detergent solution, according to ISO 106-C06: 2010. Each wash lasted 20 min, and between washes, the washing solution was renewed. After performing this procedure, the textiles substrates were again subjected to the Rh-B photodegradation process.

The photodegradation of crude oil was carried out using a wooden box equipped with a lamp (300 W) fixed at its top, which simulated the solar spectrum. Inside this wooden box, petri dishes containing 30 mL of petroleum were distributed in a circle whose center was placed immediately below the lamp. The textile substrate (already functionalized) was placed in each of these petri dishes. Afterward, the samples were irradiated for 40 h. During this period, aliquots from the petri dishes were tested after 10, 20, and 40 h for later analysis by Synchronous Fluorescence Spectroscopy (SFS) using a spectrofluorimeter (SPEX 1934D Phosphorimeter) equipped with a Xenon lamp and a Rhodamine marker.

Unlike usual luminescence spectroscopy, where the emission wavelength (λ_{em}) is fixed and the excitation wavelength (λ_{exc}) is scanned (i.e., a fluorescence excitation spectrum) or the excitation wavelength (λ_{exc}) is fixed, and the emission wavelength (λ_{em}) is scanned to get a plot of intensity vs. emission wavelength (i.e., a fluorescence emission spectrum), SFS comprises both the excitation and emission monochromator being scanned simultaneously, keeping a constant wavelength difference, $\Delta\lambda$. In this work, the spectra were recorded in the range from 300 to 750 nm, with a constant wavelength difference, $\Delta\lambda = 20\text{nm}$. The wavelength difference is represented as $\Delta\lambda = \lambda_{em} - \lambda_{exc}$. Fourier Transformed Infrared (Nicolet–Avatar 360) and UV–vis analysis was also performed.

Results and discussions

X-ray diffraction (XRD)

The XRD pattern of TiO_2 powder nanoparticles is shown in Fig. 1. The anatase crystalline phase is confirmed by the diffraction peaks (101), (004), and (200) while the rutile crystalline phase was identified

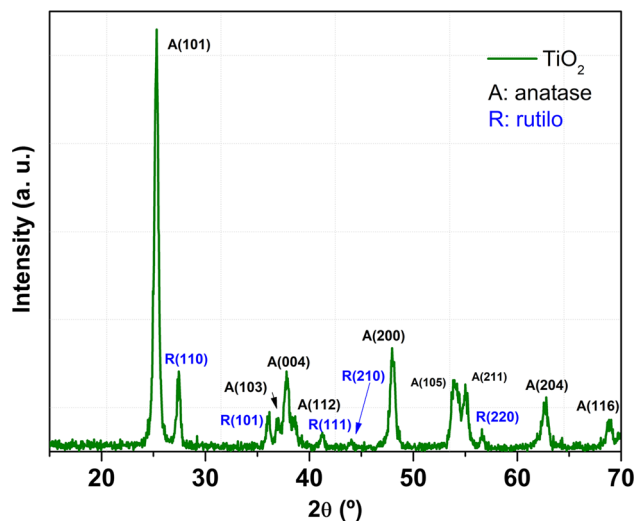


Figure 1 X-ray diffraction spectrum of TiO_2 nanoparticles.

by the diffraction peaks (110), (111), and (002). The percentage of anatase and rutile phases can be calculated from the TiO_2 powder X-ray diffractogram using Eq. 1 [24].

$$X_A = \frac{1}{\left[1 + 1.26 \left(\frac{I_R}{I_A}\right)\right]}, \quad (1)$$

Here X_A is the mass fraction of anatase, I_R is the peak intensity (110) of the rutile, and I_A is the peak intensity (101) of the anatase phase. The amount of anatase, calculated according with Eq. 1, was about 82.4%, indicating that the TiO_2 nanoparticles are predominantly composed of the anatase crystalline phase.

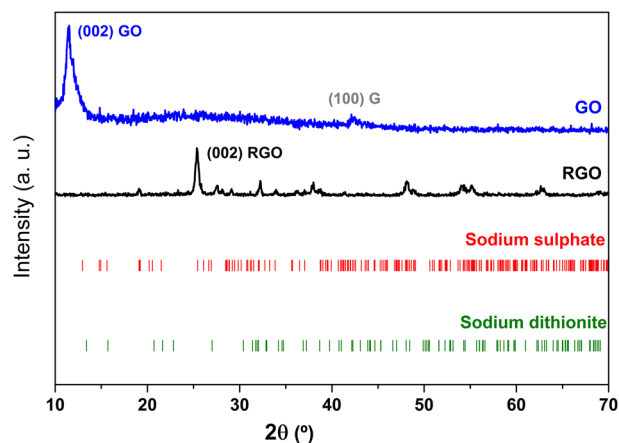


Figure 2 X-ray diffraction pattern obtained for powders RGO and GO.

On the other hand, the diffractogram presented in Fig. 2 identifies the characteristic peak of GO (002) at $2\theta = 11.52^\circ$ and another one at $2\theta = 42.12^\circ$, which is associated the carbon hexagonal structure. Analyzing the diffractogram related to the reduced graphene oxide, it is clear to observe that the characteristic peak of the GO at $2\theta = 11.52^\circ$ disappeared, and a new peak is found at the angular position of $2\theta = 25.36^\circ$. The disappearance of the peak at $2\theta = 11.52^\circ$ and the appearance of the peak at $2\theta = 25.36^\circ$ (referring to the plane (002)), suggest that the GO was reduced to RGO. Regarding the lower intensity peaks found in the RGO diffractogram, they probably result from compounds that can be formed during the GO reduction process.

Band gap energy by diffuse reflectance spectra

The UV–vis diffuse reflectance (R) of the functionalized textiles were recorded as a function of the incident photon wavelength (λ), and the data were utilized to estimate the band gap energy (E_g) of the TiO_2 nanoparticles. For this goal, the procedure widely employed consists of using the Kubelka–Munk model and the Tauc plot, which is explained in detail in [68]. Briefly, in the strong absorption edge region, the Kubelka–Munk function, $F(R)$, defined by Eq. 2, can be considered proportional to the absorption coefficient (α) of material, that is, $F(R) \propto \alpha$. The Kubelka–Munk function can be expressed by the following equation:

$$F(R) = \frac{(1 - R)^2}{2R} \tag{2}$$

Here R is the reflectance of the material, and its absorption coefficient (α) is related to the incident photon energy ($E = 1239.7/\lambda$) by the equation

$$\alpha(E) = B \frac{(E - E_g)^n}{E} \tag{3}$$

In Eq. 3, B is an independent parameter of photon energy (E), and the value of the exponent n depends on the electronic transition type involving the valence and conduction bands of the semiconductor material [69]. Therefore, the E_g values can be obtained by extrapolating to the energy axis a linear fit to a plot of $(F(R) \times E)^{1/n}$ versus E (Tauc plot). Figure 3 shows a

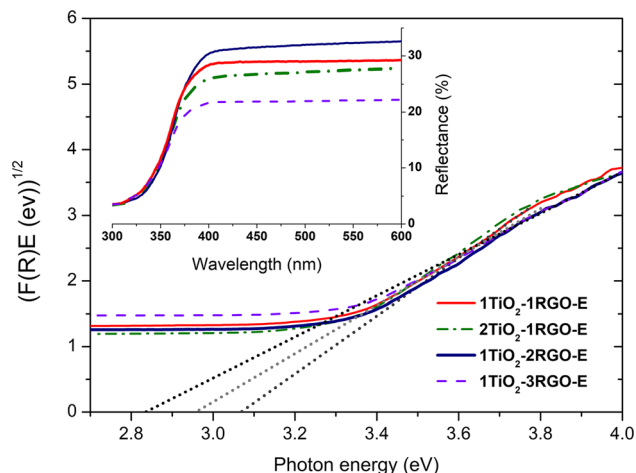


Figure 3 Tauc’s plot for Entretela functionalized at different treatments; the inset is the corresponding UV–vis diffuse reflectance spectra.

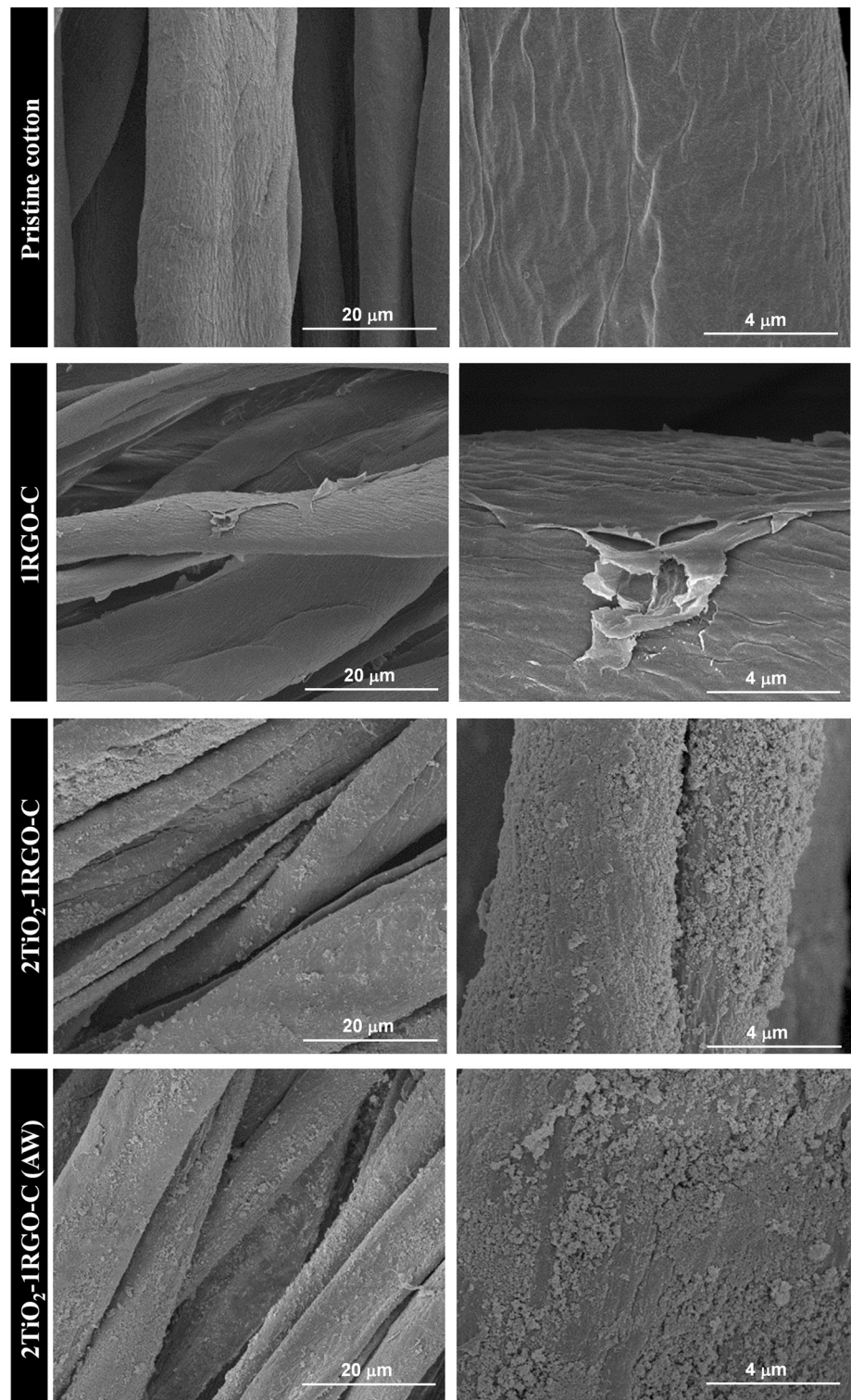
Table 1 Indirect band gap values (in eV) for TiO_2 nanoparticles deposited onto different textiles substrates previously coated with reduced graphene oxide

Treatment	E_g (eV)		
	Cotton	Entretela	PLA
(1 or 2) TiO_2 -1RGO	3.14	3.07	3.03
(1 or 2) TiO_2 -2RGO	3.13	2.92	2.94
(1 or 2) TiO_2 -3RGO	3.02	2.83	2.94

typical diffuse reflectance spectra (inset) and the corresponding Tauc plot.

Table 1 presents the E_g values assuming an indirect transition-type for TiO_2 nanoparticles. In the present work, the obtained results revealed that for the samples previously functionalized with RGO coatings, the application of one or two coatings of TiO_2 do not significantly change the value of E_g . However, in general, there was a decrease in the E_g values with the increase in the number of RGO coatings for the synthesized hybrids on the textiles, in agreement with the literature reports [47, 53, 70]. The obtained lowest values of E_g were 3.02, 2.83, and 2.94 eV for (1 or 2) TiO_2 -3RGO hybrids over Cotton, Entretela, and PLA, respectively.

Figure 4 SEM images of pristine cotton and cotton coated with 1RGO, 2TiO₂-1RGO before and after washing (AW) at a magnification of 5,000 × (first column) and 25,000 × (second column).



Morphological and elemental composition analysis by SEM and EDX

Figure 4 shows the SEM micrographs of pristine cotton and cotton coated with 1RGO and 2TiO₂-

1RGO, before and after being submitted to the washing process. In the first line of Fig. 4, it is possible to observe some details related with the morphological characteristics of the cotton fibers at magnification of 5000 × and 25,000 ×. The second

line of Fig. 4 includes two SEM images showing a region of the cotton fibres where they appear to be covered by a stack of RGO sheets. As shown in Fig. 4, the TiO₂ nanoparticles are densely distributed on the RGO coatings before (third line) and after (fourth line) a rigorous washing process, suggesting a good adhesion between these materials.

EDX analysis allowed us to detect the presence of C, O, and Ti chemical elements, in which a typical result is shown in Fig. 5. Thus, carbon and oxygen mainly derive from the fabrics, although RGO also contributes. The major peak due to Ti is located at 4.52 eV, and it is attributed to the K_α transition, but another peak exists at 4.95 eV (K_β transition). Furthermore, from the EDX spectra, it is also possible to observe that after the washing process there was a decrease in Ti peaks, therefore indicating the loss of semiconductor nanoparticles on the sample surface. On the other hand, the increase of C and O peaks may be related to the detergent used in the washing process or to the Rh-B molecules, which cannot be entirely removed from the fibers' textiles after the washing step.

Photocatalytic efficiency by Rh-B degradation

The utilization of the photocatalytic tests using an aqueous dye solution is justified due to the short run time and the possibility of obtaining a low cost clean surface after washing the textiles. The absorbance

spectra of the Rh-B dye solution are related with the variation (over time) of its concentration, *C*. At low concentrations and for a specific instant of time, *t* the absorbance intensity of the Rh-B dye solution, *A_t* is related to its solution's concentration via the Beer-Lambert law, that is, $A_t = \epsilon l C_t$, where ϵ is the molar extinction coefficient, *l* is the light path length, and *C_t* is the dye's solution concentration at a particular instant of time (light on). Therefore, by monitoring (over time) the intensity variation of the maximum absorption peak (around 564 nm) of the Rh-B dye solution, the Rh-B photodegradation efficiency, η can be calculated according to the following equation [24]:

$$\eta(\%) = (1 - A_t/A_0) \times 100, \quad (4)$$

where *A₀* is the maximum absorption peak at the initial time.

The absorbance of the Rh-B solution treated with the different functionalized samples was carried out in order to confirm the adhesion of the TiO₂-RGO system onto textiles substrates. Figure 6 shows the photocatalytic efficiency, $\eta(\%)$ curves before and after the washing process of some test samples. It can be observed that after the fabric washing process, photocatalytic efficiency presented lower values; this behavior is probably due to the washing process, which is to a quite aggressive action. Once five washes were performed at a temperature of 60 °C, this process promoted the partial removal of TiO₂ nanoparticles, according to the results shown in the EDX spectroscopy. However, it is important to notice that the photocatalytic efficiency decreased less than 12% after the rigorous washing, indicating a good immobilization of the semiconductor nanoparticles on the textile substrates, as suggested by SEM micrographs.

By using the absorbance data of the produced samples (before and after the washing process), it is possible to determine the apparent reaction rate constant, *k*, for the Rh-B dye. The *k* values were calculated according to the Langmuir–Hinshelwood (LH) model, which is explained in detail in [71]. Figure 7 shows the obtained results from the kinetic study of TiO₂ nanoparticles, immobilized on three different textile substrates comprising one or two RGO coatings. The different values for the apparent reaction rate constant, *k*, which indicates the reaction velocity, are presented in Table 2. These values were

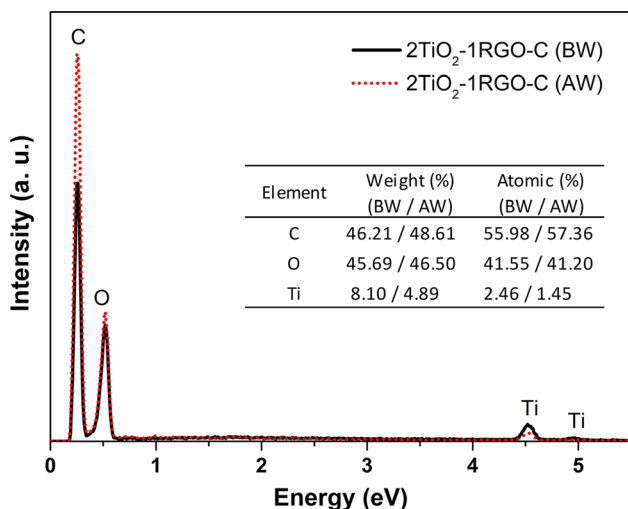
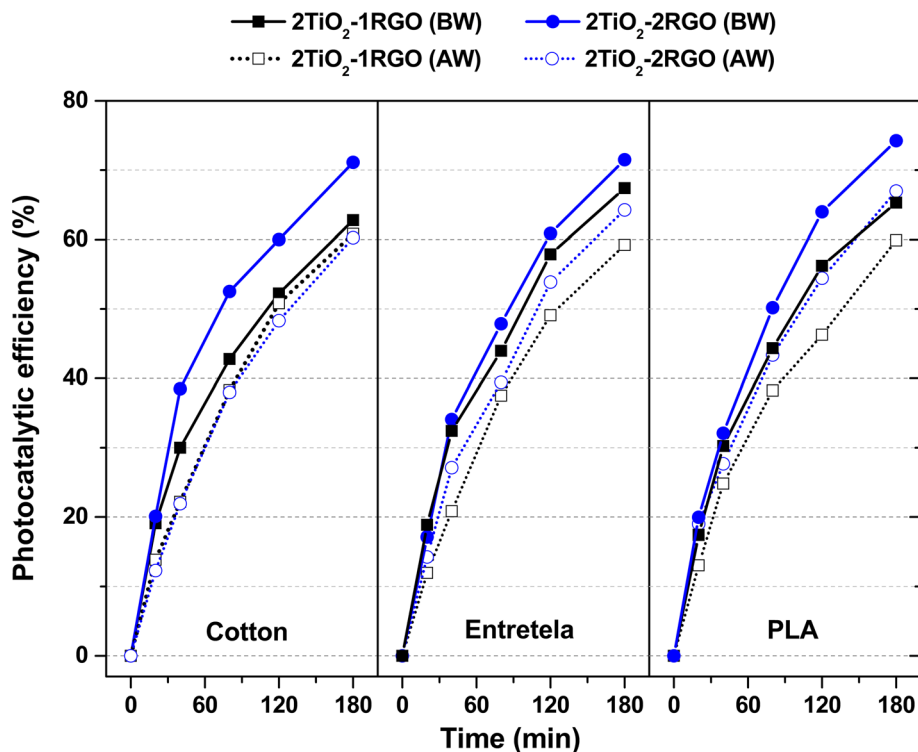


Figure 5 EDX spectra and C, O, and Ti distribution map elements for the 2TiO₂-1RGO-C sample before washing (BW) and after washing (AW) process.

Figure 6 Photocatalytic efficiencies for Rh-B degradation before and after washing (AW) of functionalized textiles. Experimental conditions: 35 °C, $[\text{Rh-B}]_{\text{initial}} = 5.0$ ppm, $V_{\text{solution}} = 400$ mL, and $\text{pH}_{\text{initial}} = 5.9$.



calculated by the angular coefficient (or slope) from the linear fitting of $\ln \frac{C_t}{C_0}$ versus time.

From the slopes of the obtained Hinshelwood plots and the summarized Table 2, the best k -values were achieved for the samples 2TiO₂-2RGO (BW) [0.00653–0.00690 min⁻¹]. After washing (AW), some particles are removed and, consequently, there is a decrease in the photocatalytic efficiency and k -value. Moreover, after washing, the sample comprising two RGO coatings (2TiO₂-2RGO) presents the best results when compared to the sample with a single RGO coating (2TiO₂-1RGO), excluding the cotton textile material. It is also observed that the Entretela substrate presented the highest k -values, regardless of treatment and (before and after) the washing condition, except for the sample 2TiO₂-1RGO (AW), which had the second highest k -value.

Photodegradation of petroleum over time by synchronous fluorescence spectroscopy

Before starting the photocatalytic tests, the oil absorbance measurements were performed in order to evaluate the light source's influence. For this purpose, the oil was exposed to light irradiation for 40 h, and its UV–vis absorbance spectrum was compared

to the spectrum of the non-irradiated sample, as shown in Fig. 8.

As can be observed, or both conditions (before and after irradiation), the shape of the absorption curve remains relatively unchanged, and the fraction of absorbed light for wavelengths above 300 nm increases slightly after exposure to light for 40 h. Therefore, based on these results, in the following discussion it will be considered that the irradiation process has a negligible influence on the molecular structure of the petroleum constituents. In terms of composition, petroleum is a complex material, as it contains aliphatic, aromatic, and macromolecular (also dense) components such as asphaltenes. From Fig. 8, it is also possible to observe two bands at 310 and 330 nm, which can be designed to a $\pi \rightarrow \pi^*$ electronic transitions in conjugated aromatic structures [72]. The exponential decay profile is due to the intense light scattering in wavelength less than 400 nm caused by asphaltene macromolecules present in the sample [73]. In addition, a possible explanation for the slight increase in the fraction of light absorbed after 40 h of irradiation involves a process of evaporation of the compounds with lower boiling points. In this context, the loss of the lighter aliphatic compounds (which do not absorb in the analyzed spectral range) and monoaromatic

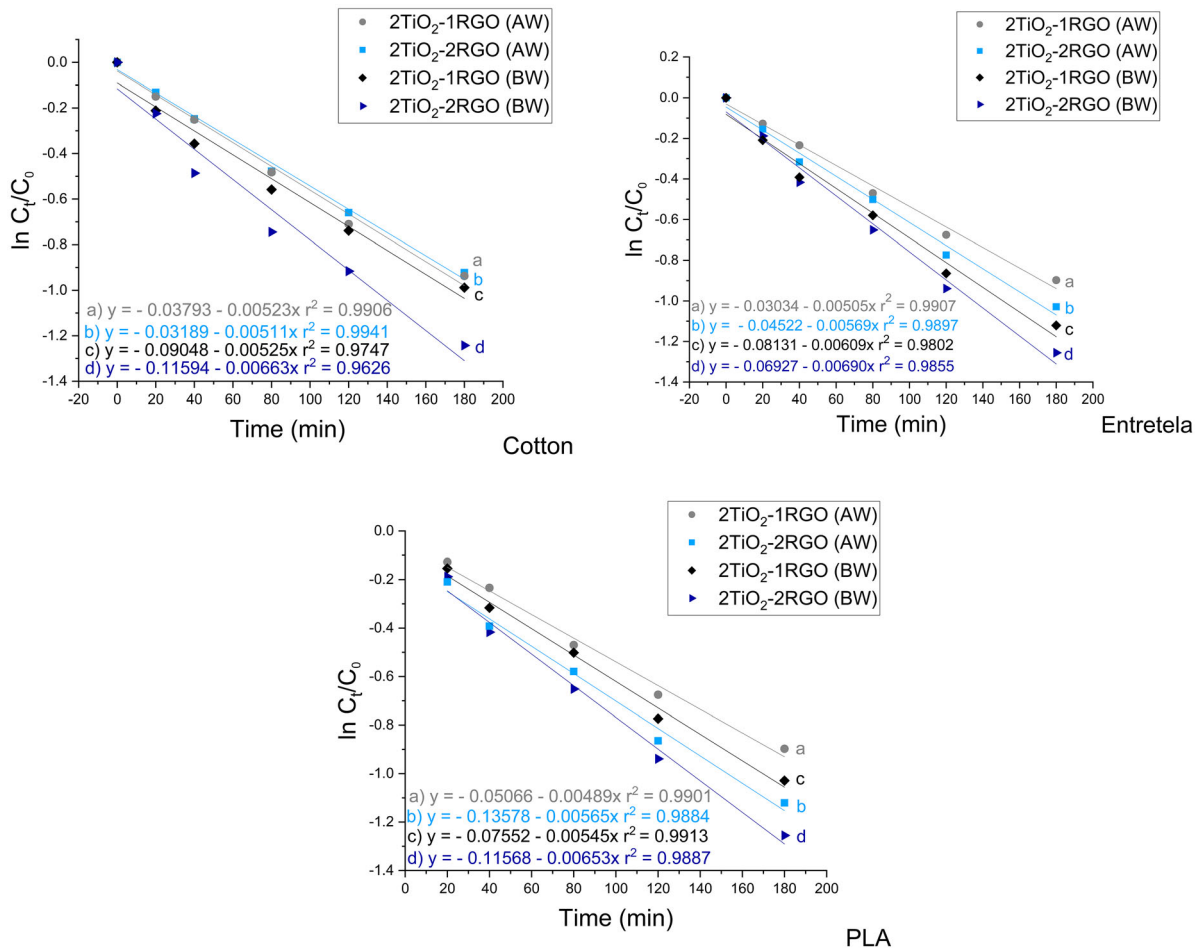


Figure 7 Typical Hinshelwood plots obtained from the results of photocatalytic efficiencies for Rh-B degradation, before and after washing of the functionalized textiles.

Table 2 Reaction rate k -values (min^{-1}) calculated from the slopes of the fitting lines for the three types of textiles materials (Cotton, Entretela, and PLA)

Textile	2TiO ₂ -1RGO (AW)	2TiO ₂ -1RGO (BW)	2TiO ₂ -2RGO (AW)	2TiO ₂ -2RGO (BW)
Cotton	0.00523	0.00525	0.00511	0.00663
Entretela	0.00505	0.00609	0.00569	0.00690
PLA	0.00489	0.00545	0.00565	0.00653

compounds with lower boiling point (which absorb with less intensity) increases the concentration of chemical components with absorption above 300 nm.

Synchronous fluorescence spectroscopy of excitation/emission was used to study the photodegradation of petroleum over time. Figure 9 exhibits the fluorescence spectra of photodegraded oil as a function of the irradiation time in the presence of functionalized textile substrates when compared to spectrum by oil without irradiation (continuum lines). In general, there is a decrease in the fluorescence intensity (non-linearly across the spectrum),

denoting that some components are very reactive and preferably destroyed [4].

Determining the relative intensity of oil fluorescence allows the study of the contribution of PAHs and polar phases over time; for this, the ratio between the fluorescence intensities at 550 nm and 350 nm (relative intensity = I_{550}/I_{350}), respectively, is taken. The observed results for the oil degradation kinetics at wavelengths of 350 nm and 550 nm are presented in Fig. 10, whose lines represent B-spline functions that were adjusted by the OriginPro software used in this research work.

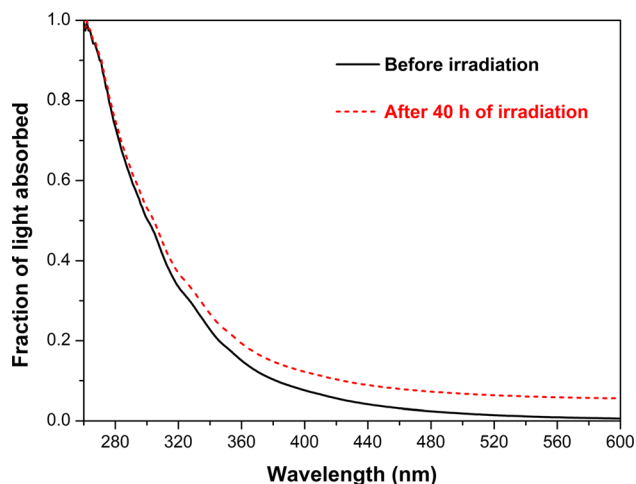
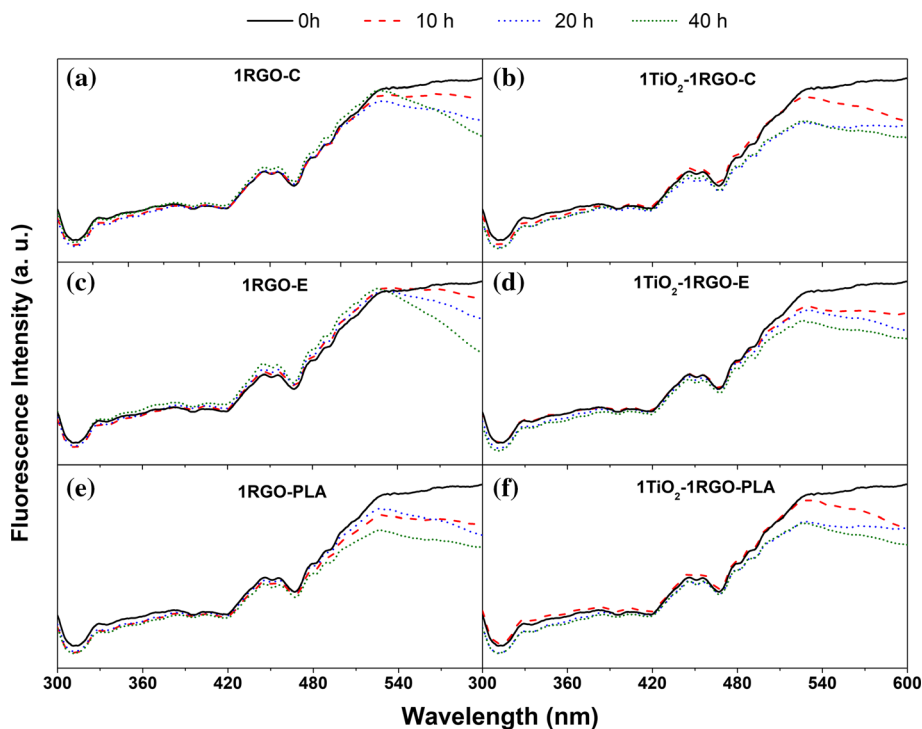


Figure 8 Fraction of light absorbed *versus* wavelength (nm). The continuum line represents the spectrum by oil without irradiation and the dashed line after 40 h of similar sunlight irradiation. The oil samples were diluted in dichloromethane in a ratio of 1:1000 (v/v) (petroleum: dichloromethane).

The selection of these wavelengths results from the possible degradation of certain species such as PAHs or fluorescent derivatives and polar phases. PAHs or fluorescent derivatives emit in a range of wavelengths from 350 to 400 nm, and the polar phases emit at approximately 550 nm [74]. Thus, it appears that, over time, there is a decrease in the contribution

Figure 9 Comparison of synchronous fluorescence spectra of photodegraded oil in the presence of functionalized textile substrates and crude oil (1:750 v/v, petroleum/dichloromethane).



of the oil's polar compounds. As they are often oxygen, nitrogen, and sulphur, containing derivatives more susceptible to undergo photoinduced molecular degradation, it is also possible to observe that the photodegradation kinetic is more significant for samples functionalized with the TiO₂-RGO system.

Fourier-transform infrared spectroscopy (FTIR)

After the oil photodegradation promoted by the action of functionalized textile substrates, a FTIR spectrum was obtained for the samples irradiated overtime. Figure 11 shows the FTIR spectra of non-treated petroleum (a) and (b) treated-petroleum with different textile substrates coated with 1TiO₂-1RGO after 40 h of light irradiation.

Analysis of the FTIR spectra suggests that the functional groups C = O and –OH represent phenols, carboxylic acids similar compounds arising from photodegradation promoted by functionalized textile substrates. The broadband appearing in the range of 3600–3200 cm⁻¹ can be attributed to the stretching vibration of hydroxyl groups, ν(OH), related to carboxylic acids and phenol derivatives [75]. In Fig. 11a and b, the bands found at 2931 cm⁻¹ and 2869 cm⁻¹ are related to the stretching modes of ν(C–H) of –CH₂ and –CH₃ groups, respectively, denoting the

Figure 10 Relative intensity of synchronous fluorescence spectra of oil-treated and non-treated at 350 and 550 nm. 1:750 v/v, petroleum/dichloromethane.

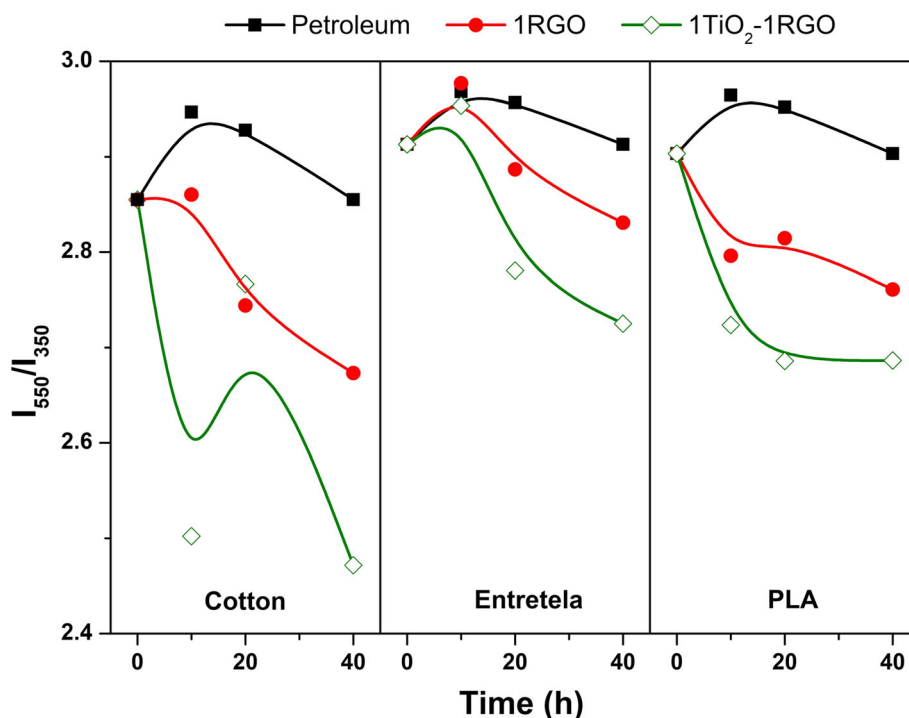
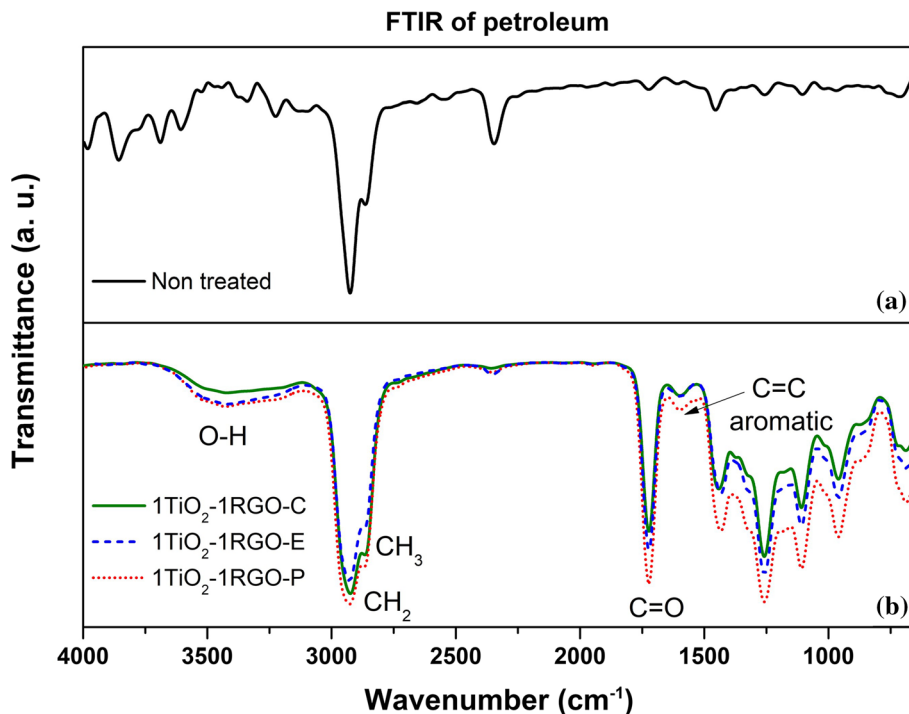


Figure 11 FTIR spectra, **a** petroleum without any treatment and **b** treated-petroleum (1:750 v/v, petroleum/dichloromethane) with functionalized textile substrates with 1TiO₂-1RGO after 40 h of irradiation in which the solid, dash, and dot lines refer to the Cotton, Entretela, and PLA textile substrates, respectively.



presence of aliphatic hydrocarbon moieties in both non-treated and thread samples. The sharp band at 1720 cm⁻¹ results from the stretching vibration of the carboxyl groups $\nu(C=O)$ of carboxylic acids. The appearance of the carboxyl band and the hydroxyl and C-O bands confirm the photoinduced oxidation

of the molecules present in the petroleum samples. The bands at the 1600–1450 cm⁻¹ region can be related to the ring stretching vibration for polyaromatic constituents. The bands at 1250–950 cm⁻¹ are related to the C–H in-plane and out-of-plane deformation modes in highly substituted aromatic rings.

The band at 1250 cm^{-1} is characteristic of the C–O stretching mode of phenols and carboxylic acids. The simplest explanation for the increase in this absorption intensity involves the formation of C–O bonds due to photochemical oxidation [4].

The functional groups present in the oil samples can also be studied by calculating the functional index of groups identified in the FTIR spectra. This calculation is performed by taking the ratio of the band area of interest and the total area of the spectrum [55]. In this way, the content of certain functional groups (related to the functional index) of untreated oil samples and oil samples subjected to photodegradation tests in the presence of functionalized textile substrates was determined as shown in Fig. 12.

As can be observed in Fig. 12, for all samples exposed to light, the formation of OH bonds occurs over the irradiation time. The 1TiO₂-1RGO-E sample promotes the most significant variation on the formation of this group after 40 h of photodegradation, which may indicate an increase in the formation of polar groups (related to petroleum degradation). On the other hand, when compared to untreated petroleum, one can observe a significant reduction in the contribution of CH₂ groups, which is related to the breaking of bonds involving this functional group. For cotton and PLA textile substrates, there is a slight

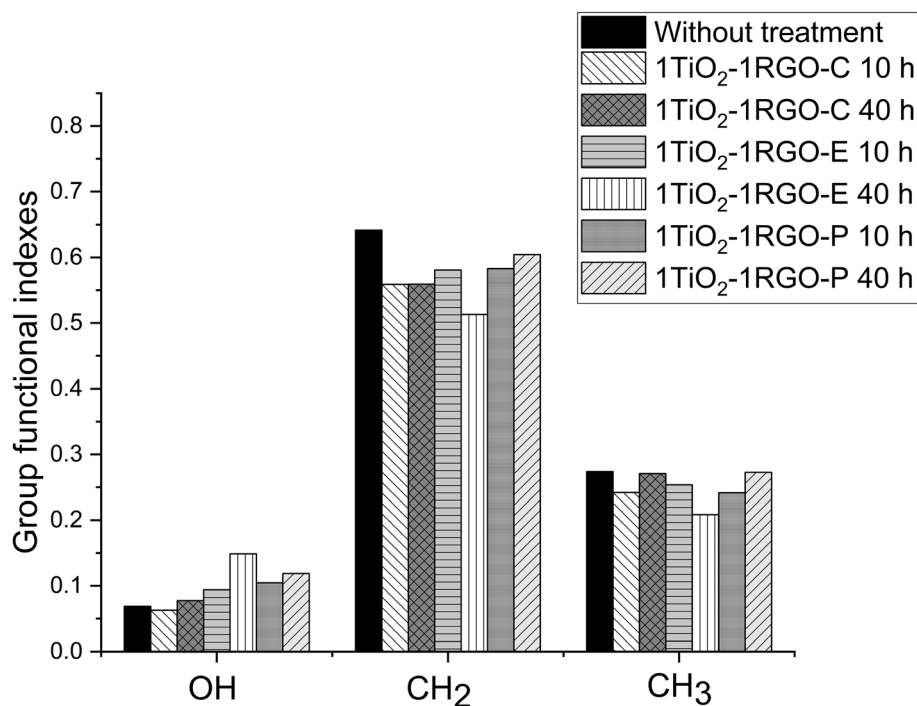
increase in the index values, from 10 to 40 h of irradiation, while for the Entretela substrate the index values decrease after completing the treatment. This evidences that the functionalized Entretela substrate was more efficient in the process of breaking CH₂ bonds. The same behavior is observed for the bonds of CH₃ groups.

Conclusions

This research work intended to study the performance of three textile substrates (Cotton, Entretela, and PLA) functionalized with the TiO₂-RGO composite material, regarding their ability to promote the photocatalytic degradation of crude petroleum under simulated sunlight irradiation. Based on the results, it can be concluded that:

- One or two coatings of TiO₂ semiconductor material do not significantly change the E_g , but there was a decrease in this parameter with the increase of RGO coatings. The obtained lowest value for E_g was 2.86 eV for (1 or 2) TiO₂-3RGO hybrids over PLA;
- SEM micrographs showed the formation of homogeneous coatings on the fabrics and the presence

Figure 12 Calculated group functional indexes of OH, CH₂, and CH₃ for the untreated petroleum samples and petroleum samples in the presence of textiles coated with 1TiO₂-1RGO after 10 and 40 h of irradiation.



of particles even after the rigorous washing process;

- Good adhesion of TiO₂ on RGO was confirmed by EDX and photocatalytic degradation of Rh-B before and after the rigorous washing process. The functionalized textiles presented high photocatalytic efficiency, decreasing less than 12% after the rigorous washing, and showing excellent dispersion and adhesion of nanoparticles around 60% (atomic % Ti) after washing.
- The results of the UV–Vis diffuse reflectance spectra showed that as TiO₂ was associated with RGO, the absorbance in the visible region of the electromagnetic spectrum increased, which may suggest a greater photocatalytic activity. This fact was confirmed by the decrease in the intensity of fluorescence synchronous spectra of crude petroleum;
- From the analysis of the FTIR spectra, it was noticed that there is the formation of OH bonds over time from exposure to light, which may indicate the increased formation of polar groups (petroleum degradation).
- In order to promote the photodegradation of crude petroleum, the most suitable functionalized textile substrate was Entretela. This textile substrate presented the best results for indirect band gap values, Langmuir–Hinshelwood *k*-values, and FTIR. Besides, it is biodegradable, increasing the sustainable features of the final product.

This innovative research work demonstrates that the functionalized textiles substrates have a great potential for photocatalytic degradation of organic compounds, which promises applications in areas such as petroleum and wastewater treatment. Thus, this environmentally friendly, sustainable, and inclusive material can contribute to the transition to the novel socio-economic model recognized as “Green Recovery” since these functionalized textiles can be related to the field of clean technologies.

Acknowledgements

This work was supported by the Portuguese Foundation for Science and Technology (FCT) in the framework of the Strategic Funding UID/FIS/04650/2019 and the project PTDC/FIS-MAC/6606/2020. Also, the third author would like to acknowledge the

FCT for the Ph.D. scholarship (SFRH/BD/137421/2018). Moreover, the authors would like to acknowledge Sociedade Nacional de Combustíveis de Angola (Sonangol), which partially provided the crude oil samples.

References

- [1] D Kukkar A Rani V Kumar 2020 Recent advances in carbon nanotube sponge-based sorption technologies for mitigation of marine oil spills J Colloid Interf Sci 570 411 422 <https://doi.org/10.1016/j.jcis.2020.03.006>
- [2] D Wang W Guo S Kong T Xu 2020 Estimating offshore exposure to oil spill impacts based on a statistical forecast model Mar Pollut Bull 156 111213 <https://doi.org/10.1016/j.marpolbul.2020.111213>
- [3] ERL Tiburtius P Peralta-Zamora ES Leal 2004 Contaminação de águas por BTXs e processos utilizados na remediação de sítios contaminados Quim Nova 27 441 446 <https://doi.org/10.1590/S0100-40422004000300014>
- [4] DE Nicodem CLB Guedes RJ Correa 1998 Photochemistry of petroleum Mar Chem 63 93 104 [https://doi.org/10.1016/S0304-4203\(98\)00053-X](https://doi.org/10.1016/S0304-4203(98)00053-X)
- [5] ORS Rocha da RF Dantas MMB Duarte 2010 Oil sludge treatment by photocatalysis applying black and white light Chem Eng J 157 80 85 <https://doi.org/10.1016/j.cej.2009.10.050>
- [6] Y Chen L Zhu R Zhou 2007 Characterization and distribution of polycyclic aromatic hydrocarbon in surface water and sediment from Qiantang River, China J Hazard Mater 141 148 155 <https://doi.org/10.1016/j.jhazmat.2006.06.106>
- [7] A Songsasen S Bangkedphol HE Keenan 2002 Synchronous fluorescence spectroscopic technique: the tool for rapid identification of polycyclic aromatic hydrocarbons (PAHs) at sub-ppm level in liquid samples Nat Sci 36 301 311
- [8] SM King PA Leaf AC Olson 2014 Photolytic and photocatalytic degradation of surface oil from the Deepwater Horizon spill Chemosphere 95 415 422 <https://doi.org/10.1016/j.chemosphere.2013.09.060>
- [9] NH Alias J Jaafar S Samitsu 2018 Photocatalytic degradation of oilfield produced water using graphitic carbon nitride embedded in electrospun polyacrylonitrile nanofibers Chemosphere 204 79 86 <https://doi.org/10.1016/j.chemosphere.2018.04.033>
- [10] R Kavitha PM Nithya S Girish Kumar 2020 Noble metal deposited graphitic carbon nitride based heterojunction photocatalysts Appl Surf Sci 508 145142 <https://doi.org/10.1016/j.apsusc.2019.145142>

- [11] R Kavitha SG Kumar 2020 Review on bimetallic-deposited TiO₂: preparation methods, charge carrier transfer pathways and photocatalytic applications Chem Pap 74 717 756 <https://doi.org/10.1007/s11696-019-00995-4>
- [12] R Kavitha SG Kumar 2019 A review on plasmonic Au-ZnO heterojunction photocatalysts: preparation, modifications and related charge carrier dynamics Mater Sci Semicond Process 93 59 91 <https://doi.org/10.1016/j.mssp.2018.12.026>
- [13] A Fujishima X Zhang 2006 Titanium dioxide photocatalysis: present situation and future approaches Comptes Rendus Chim 9 750 760 <https://doi.org/10.1016/j.crci.2005.02.055>
- [14] L Pereira R Pereira CS Oliveira 2013 UV/TiO₂ photocatalytic degradation of xanthene dyes Photochem Photobiol 89 33 39 <https://doi.org/10.1111/j.1751-1097.2012.01208.x>
- [15] S Morales-Torres LM Pastrana-Martínez JL Figueiredo 2013 Graphene oxide-P25 photocatalysts for degradation of diphenhydramine pharmaceutical and methyl orange dye Appl Surf Sci 275 361 368 <https://doi.org/10.1016/j.apsusc.2012.11.157>
- [16] JO Carneiro V Teixeira P Carvalho S Azevedo 2011 Self-cleaning smart nanocoatings Nanocoatings and ultra-thin films Woodhead Publishing 397 413
- [17] F Soleimani A Nezamzadeh-Ejhiéh 2020 Study of the photocatalytic activity of CdS–ZnS nano-composite in the photodegradation of rifampin in aqueous solution J Mater Res Technol 9 16237 16251 <https://doi.org/10.1016/j.jmrt.2020.11.091>
- [18] S Ghattavi A Nezamzadeh-Ejhiéh 2019 A brief study on the boosted photocatalytic activity of AgI/WO₃/ZnO in the degradation of methylene blue under visible light irradiation Desalin Water Treat 166 92 104 <https://doi.org/10.5004/dwt.2019.24638>
- [19] H Derikvandi A Nezamzadeh-Ejhiéh 2017 Synergistic effect of p-n heterojunction, supporting and zeolite nanoparticles in enhanced photocatalytic activity of NiO and SnO₂ J Colloid Interf Sci 490 314 327 <https://doi.org/10.1016/j.jcis.2016.11.069>
- [20] B Dai M Xuan Y Lv 2019 Molten salt synthesis of Bi₂WO₆ powders and its visible-light photocatalytic activity Mater Res <https://doi.org/10.1590/1980-5373-mr-2019-0311>
- [21] N Pourshirband A Nezamzadeh-Ejhiéh 2021 An efficient Z-scheme CdS/g-C₃N₄ nano catalyst in methyl orange photodegradation: focus on the scavenging agent and mechanism J Mol Liq 335 116543 <https://doi.org/10.1016/j.molliq.2021.116543>
- [22] A Yousefi A Nezamzadeh-Ejhiéh M Mirmohammadi 2021 SnO₂-BiVO₄ mixed catalyst: characterization and kinetics study of the photodegradation of phenazopyridine Environ Technol Innov 22 101433 <https://doi.org/10.1016/j.eti.2021.101433>
- [23] S Landi Jr J Carneiro P Parpot 2021 Performance of self-cleaning cotton textiles coated with TiO₂, TiO₂-SiO₂ and TiO₂-SiO₂-HY in removing Rhodamine B and Reactive Red 120 dyes from aqueous solutions Desalin WATER Treat 223 447 455 <https://doi.org/10.5004/dwt.2021.27159>
- [24] JO Carneiro S Azevedo F Fernandes 2014 Synthesis of iron-doped TiO₂ nanoparticles by ball-milling process: the influence of process parameters on the structural, optical, magnetic, and photocatalytic properties J Mater Sci 49 7476 7488 <https://doi.org/10.1007/s10853-014-8453-3>
- [25] HSM Tabaei M Kazemini M Fattahi 2012 Preparation and characterization of visible light sensitive nano titanium dioxide photocatalyst Sci Iran 19 1626 1631 <https://doi.org/10.1016/j.scient.2012.07.005>
- [26] L-L Tan W-J Ong S-P Chai AR Mohamed 2013 Reduced graphene oxide-TiO₂ nanocomposite as a promising visible-light-active photocatalyst for the conversion of carbon dioxide Nanoscale Res Lett 8 465 <https://doi.org/10.1186/1556-276X-8-465>
- [27] WL Ong M Gao GW Ho 2013 Hybrid organic PVDF–inorganic M–rGO–TiO₂ (M = Ag, Pt) nanocomposites for multifunctional volatile organic compound sensing and photocatalytic degradation–H₂ production Nanoscale 5 11283 <https://doi.org/10.1039/c3nr03276k>
- [28] LM Pastrana-Martínez S Morales-Torres V Likodimos 2012 Advanced nanostructured photocatalysts based on reduced graphene oxide–TiO₂ composites for degradation of diphenhydramine pharmaceutical and methyl orange dye Appl Catal B Environ 123–124 241 256 <https://doi.org/10.1016/j.apcatb.2012.04.045>
- [29] A Ali M Shoeb Y Li 2021 Enhanced photocatalytic degradation of antibiotic drug and dye pollutants by graphene-ordered mesoporous silica (SBA 15)/TiO₂ nanocomposite under visible-light irradiation J Mol Liq 324 114696 <https://doi.org/10.1016/j.molliq.2020.114696>
- [30] K Pillai 2021 Single crystalline rutile TiO₂ nanorods synthesis by onestep catalyst-free vapor transport method Solid State Commun 333 114342 <https://doi.org/10.1016/j.ssc.2021.114342>
- [31] AN Ejhiéh M Khorsandi 2010 Photodecolorization of eriochrome black T using NiS–P zeolite as a heterogeneous catalyst J Hazard Mater 176 629 637 <https://doi.org/10.1016/j.jhazmat.2009.11.077>
- [32] H Zabihi-Mobarakeh A Nezamzadeh-Ejhiéh 2015 Application of supported TiO₂ onto Iranian clinoptilolite nanoparticles in the photodegradation of mixture of aniline and 2, 4-dinitroaniline aqueous solution J Ind Eng Chem 26 315 321 <https://doi.org/10.1016/j.jiec.2014.12.003>
- [33] JO Tijani OO Fatoba G Madzivire LF Petrik 2014 A review of combined advanced oxidation technologies for the

- removal of organic pollutants from water Water Air Soil Pollut 225 2102 <https://doi.org/10.1007/s11270-014-2102-y>
- [34] A Buthiyappan AR Abdul Aziz WMA Wan Daud 2016 Recent advances and prospects of catalytic advanced oxidation process in treating textile effluents Rev Chem Eng 32 1 47 <https://doi.org/10.1515/revce-2015-0034>
- [35] A Nezamzadeh-Ejehieh M Karimi-Shamsabadi 2013 Decolorization of a binary azo dyes mixture using CuO incorporated nanozeolite-X as a heterogeneous catalyst and solar irradiation Chem Eng J 228 631 641 <https://doi.org/10.1016/j.ccej.2013.05.035>
- [36] A Nezamzadeh-Ejehieh M Bahrami 2015 Investigation of the photocatalytic activity of supported ZnO–TiO₂ on clinoptilolite nano-particles towards photodegradation of wastewater-contained phenol Desalin Water Treat 55 1096 1104 <https://doi.org/10.1080/19443994.2014.922443>
- [37] Z Xiong J Ma WJ Ng 2011 Silver-modified mesoporous TiO₂ photocatalyst for water purification Water Res 45 2095 2103 <https://doi.org/10.1016/j.watres.2010.12.019>
- [38] J Schneider M Matsuoka M Takeuchi 2014 Understanding TiO₂ photocatalysis: mechanisms and materials Chem Rev 114 9919 9986 <https://doi.org/10.1021/cr5001892>
- [39] KVA Kumar KP Revathy V Prathibha 2013 Structural and luminescence enhancement properties of Eu³⁺/Ag nanocrystallites doped SiO₂-TiO₂ matrices J Rare Earths 31 441 448 [https://doi.org/10.1016/S1002-0721\(12\)60301-9](https://doi.org/10.1016/S1002-0721(12)60301-9)
- [40] F Dalto I Kuźniarska-Biernacka C Pereira 2021 Solar light-induced methylene blue removal over TiO₂/AC composites and photocatalytic regeneration Nanomaterials 11 3016 <https://doi.org/10.3390/nano11113016>
- [41] H Zhang X Lv Y Li 2010 P25-graphene composite as a high performance photocatalyst ACS Nano 4 380 386 <https://doi.org/10.1021/nn901221k>
- [42] H Mahmood A Habib M Mujahid 2014 Band gap reduction of titania thin films using graphene nanosheets Mater Sci Semicond Process 24 193 199 <https://doi.org/10.1016/j.mssp.2014.03.038>
- [43] Y Zhang HM Yang S-J Park 2018 Synthesis and characterization of nitrogen-doped TiO₂ coatings on reduced graphene oxide for enhancing the visible light photocatalytic activity Curr Appl Phys 18 163 169 <https://doi.org/10.1016/j.cap.2017.12.001>
- [44] Y Gu M Xing J Zhang 2014 Synthesis and photocatalytic activity of graphene based doped TiO₂ nanocomposites Appl Surf Sci 319 8 15 <https://doi.org/10.1016/j.apsusc.2014.04.182>
- [45] E Vasilaki I Georgaki D Vernardou 2015 Ag-loaded TiO₂/reduced graphene oxide nanocomposites for enhanced visible-light photocatalytic activity Appl Surf Sci 353 865 872 <https://doi.org/10.1016/j.apsusc.2015.07.056>
- [46] VK Boukili RL Chazdon 2017 Environmental filtering, local site factors and landscape context drive changes in functional trait composition during tropical forest succession Perspect Plant Ecol Evol Syst 24 37 47 <https://doi.org/10.1016/j.ppees.2016.11.003>
- [47] M Hamandi G Berhault C Guillard H Kochkar 2017 Reduced graphene oxide/TiO₂ nanotube composites for formic acid photodegradation Appl Catal B Environ 209 203 213
- [48] T Harifi M Montazer R Dillert DW Bahnemann 2018 TiO₂/Fe₃O₄/Ag nanophotocatalysts in solar fuel production: new approach to using a flexible lightweight sustainable textile fabric J Clean Prod 196 688 697 <https://doi.org/10.1016/j.jclepro.2018.06.031>
- [49] MT Noman MA Ashraf H Jamshaid A Ali 2018 A novel green stabilization of TiO₂ nanoparticles onto cotton Fibers Polym 19 2268 2277 <https://doi.org/10.1007/s12221-018-8693-y>
- [50] M Masae L Sengyi 2018 Hydrophobic and antibacterial activity of silk textile surfaces using reduced graphene oxide (RGO) and TiO₂ coating J Mater Sci Appl Energy 7 307 316
- [51] MS Stan IC Nica M Popa 2019 Reduced graphene oxide/TiO₂ nanocomposites coating of cotton fabrics with antibacterial and self-cleaning properties J Ind Text 49 277 293 <https://doi.org/10.1177/1528083718779447>
- [52] L Karimi ME Yazdandshenas R Khajavi 2014 Using graphene/TiO₂ nanocomposite as a new route for preparation of electroconductive, self-cleaning, antibacterial and antifungal cotton fabric without toxicity Cellulose 21 3813 3827 <https://doi.org/10.1007/s10570-014-0385-1>
- [53] S Landi JO Carneiro F Fernandes 2017 Functionalization of cotton by RGO/TiO₂ to enhance photodegradation of rhodamine B under simulated solar irradiation Water Air Soil Pollut 228 335 <https://doi.org/10.1007/s11270-017-3533-z>
- [54] AA Isari A Payan M Fattahi 2018 Photocatalytic degradation of rhodamine B and real textile wastewater using Fe-doped TiO₂ anchored on reduced graphene oxide (Fe-TiO₂/rGO): characterization and feasibility, mechanism and pathway studies Appl Surf Sci 462 549 564 <https://doi.org/10.1016/j.apsusc.2018.08.133>
- [55] JOO Carneiro S Azevedo V Teixeira 2013 Development of photocatalytic asphalt mixtures by the deposition and volumetric incorporation of TiO₂ nanoparticles Constr Build Mater 38 594 601 <https://doi.org/10.1016/j.conbuildmat.2012.09.005>
- [56] M Ines P Paolo F Roberto S Mohamed 2019 Experimental studies on the effect of using phase change material in a salinity-gradient solar pond under a solar simulator Sol Energy 186 335 346 <https://doi.org/10.1016/j.solener.2019.05.011>

- [57] T Göckler S Haase X Kempter 2021 Tuning superfast curing thiol-norbornene-functionalized gelatin hydrogels for 3D bioprinting *Adv Healthc Mater* 10 1 13 <https://doi.org/10.1002/adhm.202100206>
- [58] V Baglio M Girolamo V Antonucci AS Aricò 2011 Influence of TiO₂ film thickness on the electrochemical behaviour of dye-sensitized solar cells *Int J Electrochem Sci* 6 3375 3384
- [59] L Derendorp JB Quist R Holzinger T Röckmann 2011 Emissions of H₂ and CO from leaf litter of *Sequoiadendron giganteum*, and their dependence on UV radiation and temperature *Atmos Environ* 45 7520 7524 <https://doi.org/10.1016/j.atmosenv.2011.09.044>
- [60] D Hainzl J Burhenne H Parlar 1993 Isolation and characterization of environmental relevant single toxaphene components *Chemosphere* 27 1857 1863 [https://doi.org/10.1016/0045-6535\(93\)90381-E](https://doi.org/10.1016/0045-6535(93)90381-E)
- [61] M Abdelhamid D Korte H Cabrera 2021 Thermo-optical characterization of Cu- and Zr-modified TiO₂ photocatalysts by beam deflection spectrometry *Appl Sci* 11 10937
- [62] M Özcan B Birol F Kaya 2021 Investigation of photocatalytic properties of TiO₂ nanoparticle coating on fly ash and red mud based porous ceramic substrate *Ceram Int* 47 24270 24280 <https://doi.org/10.1016/j.ceramint.2021.05.138>
- [63] I Rocha Segundo C Ferreira EF Freitas 2018 Assessment of photocatalytic, superhydrophobic and self-cleaning properties on hot mix asphalts coated with TiO₂ and/or ZnO aqueous solutions *Constr Build Mater* 166 36 44 <https://doi.org/10.1016/j.conbuildmat.2018.01.106>
- [64] B Zahabizadeh E Freitas A Cam JO Carneiro 2021 Development of photocatalytic 3D-printed cementitious mortars: influence of the curing, spraying time gaps and TiO₂ coating rates *Buildings* 11 381
- [65] IGD Rocha Segundo S Landi Jr SMB Oliveira 2019 Photocatalytic asphalt mixtures: mechanical performance and impacts of traffic and weathering abrasion on photocatalytic efficiency *Catal Today* <https://doi.org/10.1016/j.cattod.2018.07.012>
- [66] S Filice R Fiorenza R Reitano 2020 TiO₂ colloids laser-treated in ethanol for photocatalytic H₂ production *ACS Appl Nano Mater* 3 9127 9140 <https://doi.org/10.1021/acsnm.0c01783>
- [67] S Landi J Carneiro S Ferdov 2017 Photocatalytic degradation of Rhodamine B dye by cotton textile coated with SiO₂-TiO₂ and SiO₂-TiO₂-HY composites *J Photochem Photobiol A Chem* 346 60 69 <https://doi.org/10.1016/j.jphotochem.2017.05.047>
- [68] S Landi IR Segundo E Freitas 2022 Use and misuse of the Kubelka-Munk function to obtain the band gap energy from diffuse reflectance measurements *Solid State Commun* 341 114573 <https://doi.org/10.1016/j.ssc.2021.114573>
- [69] N Omrani A Nezamzadeh-Ejhih 2020 Focus on scavengers' effects and GC-MASS analysis of photodegradation intermediates of sulfasalazine by Cu₂O/CdS nanocomposite *Sep Purif Technol* 235 116228 <https://doi.org/10.1016/j.seppur.2019.116228>
- [70] J Molina F Fernandes J Fernández 2015 Photocatalytic fabrics based on reduced graphene oxide and TiO₂ coatings *Mater Sci Eng B* 199 62 76 <https://doi.org/10.1016/j.mseb.2015.04.013>
- [71] M Mehrli-Afjani A Nezamzadeh-Ejhih H Aghaei 2020 A brief study on the kinetic aspect of the photodegradation and mineralization of BiOI-Ag₃PO₄ towards sodium diclofenac *Chem Phys Lett* 759 137873 <https://doi.org/10.1016/j.cplett.2020.137873>
- [72] Malkin J 1992 Photophysical and photochemical properties of aromatic compounds CRC Press
- [73] EEB Cruz NVG Rivas UP García AMM Martínez JAM Banda 2017 Characterization of crude oils and the precipitated asphaltene fraction using UV spectroscopy, dynamic light scattering and microscopy *Recent Insights Petroleum Science Engineering IntechOpen* 117 135
- [74] K Tjessem A Aaberg 1983 Photochemical transformation and degradation of petroleum residues in the marine environment *Chemosphere* 12 1373 1394
- [75] L Bellamy 1975 The Infra-red spectra of complex molecules 1 Chapman and Hall London

Publisher's Note Springer Nature remains neutral with regard to jurisdictional claims in published maps and institutional affiliations.